Photoemission and Tunneling Spectroscopy of Topological Materials

Jian-Feng Ge#, Mengyu Yao##and Claudia Felser###

Topological materials are distinguished from trivial materials by the nontrivial topology of their electronic band structures. Therefore, analyzing these band structures is crucial for identifying and understanding topological materials. Angle-resolved photoemission spectroscopy can be used to directly determine the electronic band structure for the occupied states, while spectroscopic-imaging scanning tunneling microscopy can also access the states above the Fermi level. Here, we discuss the use of these complementary techniques to investigate topological semimetals such as $EuCd_2As_2$, MnBi, and $SrSi_2$, uncovering the Weyl physics underlying their unusual transport properties.

Topological materials have emerged as a novel class of quantum materials defined by nontrivial topological phases that remain stable against perturbations and impurities. Originating from the discovery of the quantum Hall effect, these materials include topological insulators, topological superconductors and Weyl semimetals, each hosting exotic quasiparticles and exhibiting unusual transport phenomena. Their inherent stability and unique edge states have great potential for applications in dissipationless electronics, fault-tolerant quantum computing, and spintronics.

Clarifying the electronic band structure of a material to determine its band topology is central to its topological classification. Angle-resolved photoemission spectroscopy (ARPES) and spectroscopic-imaging scanning tunneling microscopy (STM) are two of the most advanced techniques for probing band structures. In ARPES, band electrons are excited by incident photons, and their binding energies and momenta are then determined using an electron spectrometer. In STM, the scattering of band electrons by surface imperfections results in electronic density oscillations, which are imaged in real space via a tunnel current that is collected at a metallic tip with varying bias energy with respect to the Fermi level. Using the Fourier transform, the dispersion relation can be derived in momentum space. ARPES provides direct information and high momentum resolution of the band structure, whereas STM can access both occupied and unoccupied states with atomic-scale resolution.

Here, we show our recent progress on the Weyl semimetal candidates $EuCd_2As_2$, MnBi, and $SrSi_2$ using complementary ARPES and STM techniques. Weyl semimetals have attracted significant attention because of the low-energy chiral Weyl fermions predicted to exist within them, which are promising for realizing chiral anomalies. The band structure of Weyl semimetals is characterized by Weyl points, at which the bulk Fermi surface shrinks to zero. Weyl points with opposite chirality are paired and connected in momentum space by unclosed Fermi arcs [2], offering direct evidence of Weyl physics.

$EuCd_2As_2$: an ideal ferromagnetic Weyl semimetal

The Weyl semimetal phase can be realized in crystals that break time-reversal symmetry, inversion symmetry, or both. Notably, breaking time-reversal symmetry allows for the realization of a minimum of two Weyl points, with such materials exhibiting ideal Weyl semimetal behavior. These ideal Weyl semimetals are particularly favored for studying Weyl physics phenomena such as chiral anomalies and chiral Majorana modes owing to their well-defined helicity and preserved Lorentz invariance. $EuCd_2As_2$ is an excellent candidate for ideal Weyl semimetals because of its combination of magnetism and topology, as well as its Weyl fermions. However, the Weyl physics of ferromagnetic $EuCd_2As_2$ are still underexplored.

We use synchrotron-based ARPES with soft X-ray photons to accurately determine the three-dimensional band structure of $EuCd_2As_2$ on both the Γ–M–K and the Γ–K–A planes (Figure 1a) [1]. To analyze the effect of magnetic order on the band structure, we performed ARPES along the Γ–M direction both above

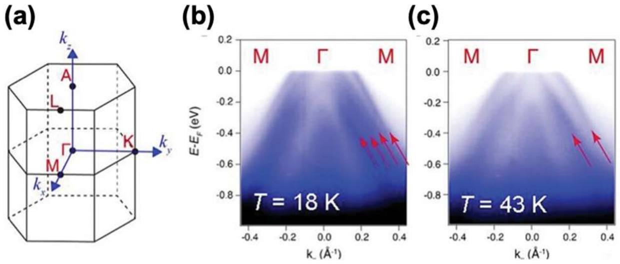

Fig. 1: ARPES data of $EuCd_2As_2$. (a) Bulk Brillouin zone of $EuCd_2As_2$ with high-symmetry points labeled. (b, c) ARPES intensity plots along the Γ–M direction measured at (b) 18 and (c) 43 K.

and below the ferromagnetic phase transition temperature. By comparing the spectra of the ferromagnetic (18 K, Figure 1b) and paramagnetic (43 K, Figure 1c) states, we observed significant differences in the band structure. This ferromagnetic transition-induced band splitting, together with our observation of cone-like band dispersion below E_F, is consistent with our density functional theory (DFT) calculations. We also observed similar changes along the Γ–A direction.

To elucidate the electronic structure of $EuCd_2As_2$ above the Fermi energy, we conducted STM experiments in collaboration with Vidya Madhavan at the University of Illinois Urbana-Champaign. The spatially resolved differential conductance maps in Figure 2a show the spatial modulation originating from interference between the band electrons.

We extracted the scattering vectors for the unoccupied states by Fourier transform, providing momentum-space information at each energy, as shown in Figure 2b for 0 meV. To obtain the dispersion relation, line cuts of the Fourier-transformed images at different energies along the Γ–M direction were stacked vertically (Figure 2c). In this material, the maximum scattering vector at the Fermi energy was equal to the Fermi wavevector k_F.

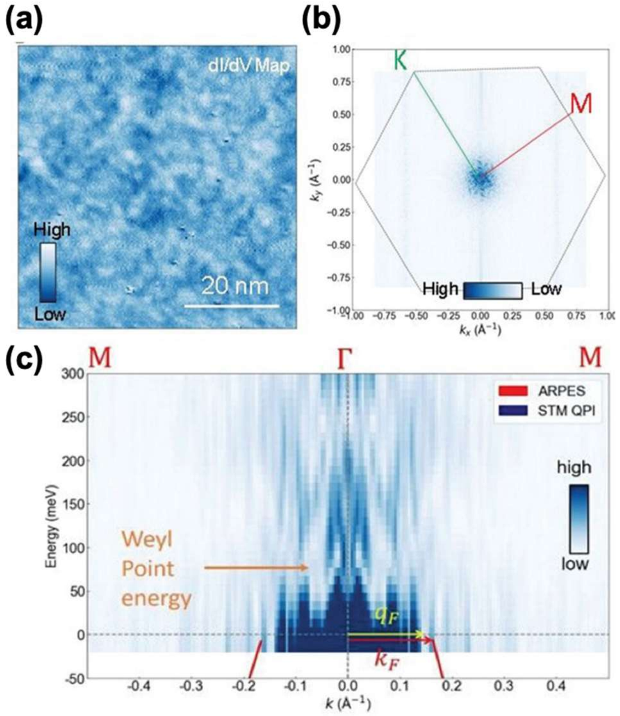

Fig. 2: Spectroscopic-imaging scanning tunneling microscopy (STM) data of $EuCd_2As_2$. (a) Spatially resolved differential conductance map. (b) Fourier transform of conductance map at 0 mV. (c) Energy–momentum linecut of quasiparticle interference along the Γ–M direction. The orange arrow indicates the expected Weyl point energy. The red solid lines indicate the dispersion from ARPES along the Γ–M direction.

These STM results can be explained by scattering between the Fermi arc states – which project densely to the Γ point on the k_x–k_y plane – and the bulk bands along the Γ–M direction. Our DFT results show that the Weyl nodes and Fermi arc states very close to the Γ point, with an in-plane component much smaller than the in-plane k_F. Therefore, the scattering from these arc states to a bulk band state shares nearly the same wavevector, and the spectroscopic intensity of this nearly degenerate scattering could be much larger than the intensity of scattering from one bulk band state to another at opposite momentum.

Our ARPES and STM investigation of the electronic structure of $EuCd_2As_2$ agreed well with our DFT calculations. This work opens new avenues for studying magnetic Weyl semimetals and boosts theoretical and experimental investigations into ideal Weyl semimetals with anomalous electrical and thermal transport.

MnBi: a ferromagnet with a large magnetoresistance

Giant magnetoresistance has garnered significant interest for its theoretical implications and commercial applications such as hard-disk read/write heads. Most ferromagnetic materials, which are typically metals, exhibit small and negative magnetoresistance owing to the presence of localized electrons in heavy *d* bands with low Fermi velocity. Substantial efforts have been directed toward discovering new ferromagnetic materials with large magnetoresistance. It has been reported that massless Weyl states in nonmagnetic Weyl semimetals can generate giant magnetoresistance at low temperatures, which is attributed to linear band crossings at the Fermi energy and high Fermi velocity. Because of the topological nature of their electronic structures, these materials exhibit suppressed backscattering and spin scattering. Therefore, ferromagnetic Weyl semimetals are promising candidates for achieving high magnetoresistance.

We discovered [2] that ferromagnetic MnBi exhibits a large linear nonsaturating magnetoresistance of 5000% under a pulsed field of 70 T with a mobility of 5000 $cm^2\ V^{-1}\ s^{-1}$ at 2 K, which is one of the highest values reported for ferromagnetic materials. The transport data of this material show two-charge-carrier

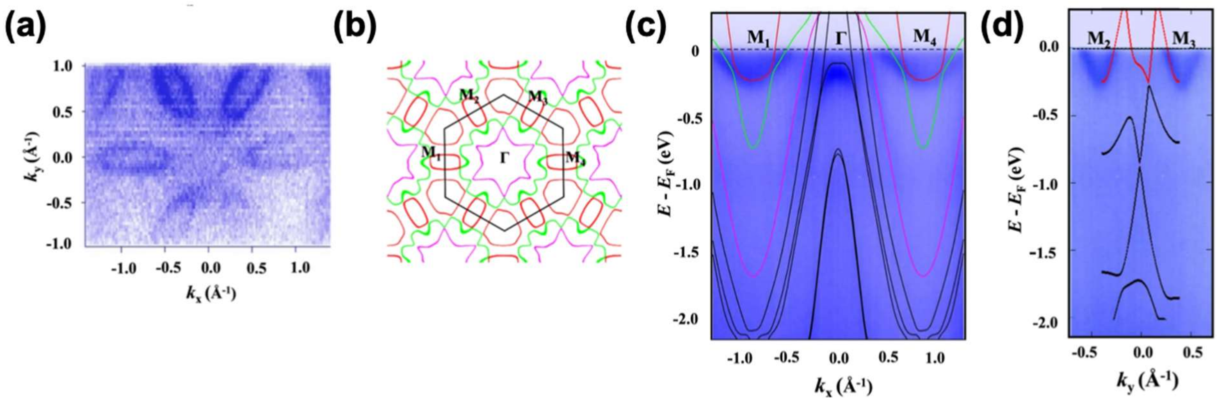

Fig. 3: Electronic structure of MnBi. (a) Fermi surface map of MnBi at $k_z = 0$. *(b) Calculated Fermi surface at* $k_z = 0$. *ARPES intensity plot along the (c)* M_1–Γ–M_4 *and (d)* M_2–M_3 *directions with calculated bands overlaid.*

behavior with a relatively low density, indicating that it has a topological band structure in momentum space.

To elucidate the origin of the unusually high mobility of MnBi, we examined its electronic structure using ARPES. The ARPES data in Figure 3a show the flower-like texture of the Fermi surface in the $k_z = 0$ plane, which agrees with the calculated Fermi surface (Figure 3b). A series of hole pockets at the Γ point are surrounded by six electron pockets at the M points, confirming its two-charge-carrier behavior. The band structure observed from the ARPES intensity plots along the M_1–Γ–M_4 and M_2–M_3 directions (Figure 3c and 3d, respectively) was consistent with our DFT results, with a rigid energy shift. By fitting the electron bands to a parabola, we find that the Fermi velocity is as high as 10.2 eV Å and the effective mass near the Fermi energy is as small as 0.42 m_e. Being inversely proportional to the mobility, this low effective mass is the origin of the high transport mobility of MnBi. Moreover, the unique topological character of the bands in MnBi, as inferred from the ARPES and DFT results, allows for a reduction in backscattering, which would increase the mobility. The linear crossings (Figure 3d) lead to a special case of electron–hole compensation that drastically enhances the mobility of magnetic systems.

$SrSi_2$: a Weyl semimetal under pressure

In contrast to the bulk bands associated with Weyl nodes, Fermi arcs are surface states that terminate at the projections of Weyl nodes with opposite chiral charges. The chiral charge of a Weyl node can be determined by counting the connected Fermi arcs. In Weyl semimetals, Weyl fermions are typically protected by either inversion or mirror symmetry. The inversion-asymmetric chiral compound $SrSi_2$ was predicted to be a robust Weyl semimetal that lacks both mirror and inversion symmetry. However, no experimental research has been conducted on $SrSi_2$ systems owing to challenges in its growth [3]. Consequently, direct evidence for the presence or absence of Weyl nodes in $SrSi_2$ remains unavailable.

We conducted a systematic ARPES study [4] of both undoped and Ca-doped $SrSi_2$ samples. The high-resolution spectrum along the Γ–X direction in the $k_z = 0$ plane (Figure 4a) showed only one hole band, which forms the Fermi surface pockets. However, no electron bands cross the hole band. The ARPES data showed excellent agreement with first-principles calculations (Figure 4b) and confirmed that the bottom of the electron bands was located above the hole band without crossing them.

Theoretically, Ca doping should shrink the $SrSi_2$ lattice and increase the overlap between the hole and electron bands. Nevertheless, the band structures of two Ca-doped $Sr_{1-x}Ca_xSi_2$ samples (x = 2% and 5%; Figure 4c and 4d, respectively) were similar to that of the undoped sample in ARPES. This work suggests that $SrSi_2$ is a trivial semiconductor at ambient pressure.

Interestingly, while no Fermi arcs or Weyl nodes were observed in the ARPES experiments at ambient pressure, our transport experiments demonstrated a semiconductor–metal transition in $SrSi_2$ under high pressure (approximately 12 GPa). This indicates the existence of Weyl nodes under pressure, which is supported by our calculations.

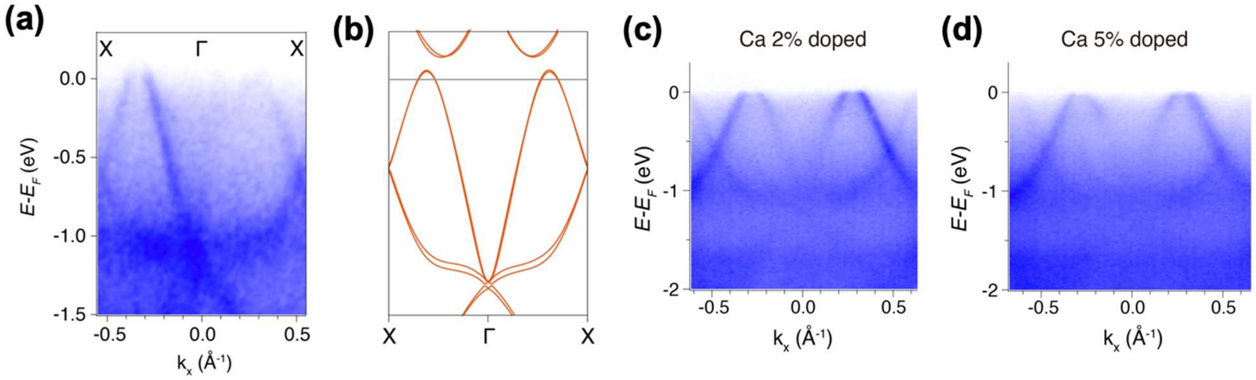

Fig. 4: Electronic structure of $SrSi_2$. (a) Photoemission intensity plot along the Γ–X direction and (b) corresponding calculated band structure. High resolution photoemission intensity plots of $Ca_xSr_{1-x}Si_2$ along the Γ–X direction for (c) x = 2% and (d) x = 5%.

Future directions

Topological semimetals present a wealth of unexplored physics. Moreover, when coupled with superconductivity (i.e., topological superconductivity), they even hold the potential to realize error-resistant quantum computing. While our current focus involves the analysis of the band structures and topological nature of these materials using ARPES and STM, our future research will place greater emphasis on the exotic quantum states harbored by these topological materials.

An example material from our ongoing research [5] is $NbGe_2$, which exhibits superconductivity below 2 K and a unique nonsymmorphic chiral crystal lattice that hosts Kramers-Weyl fermions. Our ARPES measurements have directly revealed exotic chiral surface states in $NbGe_2$ resulting from the lack of inversion and mirror symmetries, providing evidence for Weyl fermions, supported by band structure calculations. Complemented by transport measurements, our results suggest that $NbGe_2$ is a promising platform for investigating the interplay between chirality, topology, and superconductivity.

A crucial task in the field of topological superconductivity is the discovery of Majorana quasiparticles, which are fundamental components of fault-tolerant quantum computers. Despite a decade of experimental effort, conclusive evidence for their existence remains elusive, and the ability to braid them is still out of reach. New material platforms and techniques are needed to address this fundamental challenge. Notably, STM is particularly well-suited for this purpose.

Recently, a new technique known as local shot noise spectroscopy (Figure 5a) has provided a novel approach for detecting Majorana quasiparticles. By analyzing the effective charge during the tunneling process, this method identifies spectroscopic features in both noise and standard tunneling spectroscopy, suggesting a Majorana origin [6], as shown in Figure 5b. We recently utilized the raster scanning capability of STM with local shot noise spectroscopy to image atomic-scale noise in the vortex lattice (Figure 5c) of the trivial superconductor $NbSe_2$ [7]. This technique enabled the visualization of delocalized quasiparticles, aiding in the determination of the pairing symmetry. The diverse range of topological pairing symmetries promises the observation of Majorana states at atomic step edges and vortex cores.

Chiral topological superconductors, intertwined with charge orders, may host electron multiplets such as quartets and sextets, which can be directly obtained by local shot noise spectroscopy. Unlike conventional charge-2*e* superconductivity, which arises from a condensate of electron pairs, these states are formed by bound states of electron multiplets, stabilizing charge-4*e* and charge-6*e* superconductivity.

External Cooperation Partners

Ming Shi and Valdimir Strokov (Swiss Light Source, Paul Scherrer Institute); Vidya Madhavan (University of Illinois Urbana-Champaign); and Milan Allan (Leiden University and Ludwig-Maximilians-Universität München).

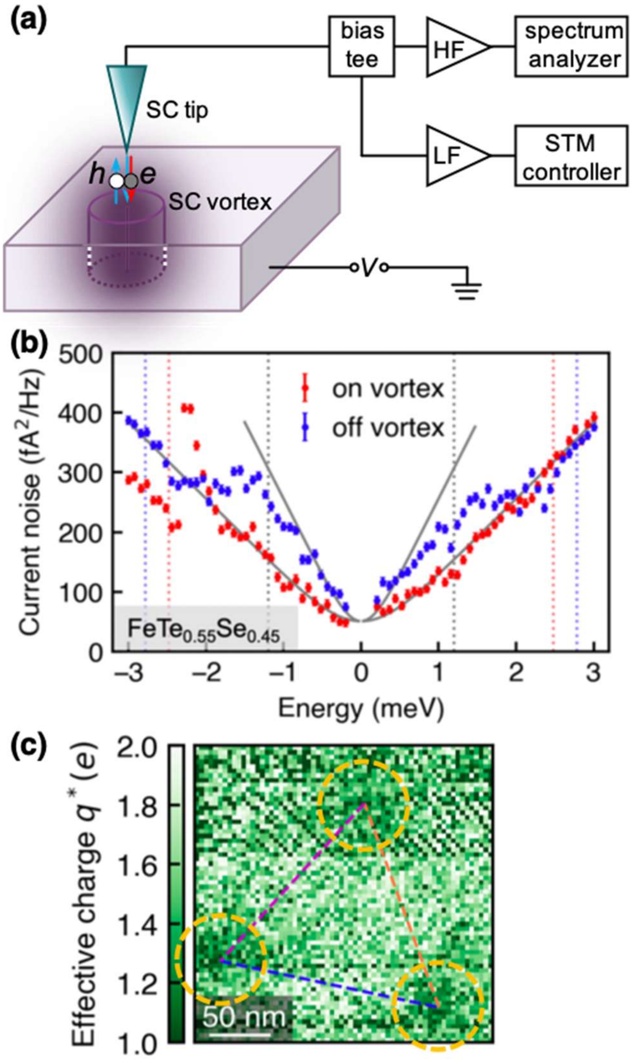

Fig. 5: Local shot noise spectroscopy. (a) Schematic illustration of the scanning tunneling noise microscope setup. (b) Current noise spectra taken on (red) and off (blue) the vortex core hosting putative Majorana quasiparticles, respectively. (c) Spatial distribution of the effective charge extracted from current noise image across three vortex cores (yellow dashed circles). A lower effective charge means more quasiparticles.

References

[1]* *Anomalous Hall conductivity and Nernst effect of the ideal Weyl semimetallic ferromagnet EuCd$_2$As$_2$, S. Roychowdhury, M. Yao, K. Samanta, S. Bae, D. Chen, S. Ju, A. Raghavan, N. Kumar, P. Constantinou, and S. N. Guin, N. C. Plumb, M. Romanelli, H. Borrmann, M. G. Vergniory, V. N. Strocov, V. Madhavan, C. Shekhar, and C. Felser, Adv. Sci.* ***10*** *(2023) 2207121,* *https://doi.org/10.1002/advs.202207121*

[2]* *Large linear non-saturating magnetoresistance and high mobility in ferromagnetic MnBi, Y. He, J. Gayles, M. Yao, T. Helm, T. Reimann, V. N. Strocov, W. Schnelle, M. Nicklas, Y. Sun, G. H. Fecher, and C. Felser, Nat. Commun.* ***12*** *(2021) 4576,* *https://doi.org/10.1038/s41467-021-24692-7*

[3]* *Three-dimensional quasiquantized Hall insulator phase in SrSi$_2$, K. Manna, N. Kumar, S. Chattopadhyay, J. Noky, M. Yao, J. Park, T. Förster, M. Uhlarz, T. Chakraborty, B. V. Schwarze, J. Hornung, V. N. Strocov, H. Borrmann, C. Shekhar, Y. Sun, J. Wosnitza, C. Felser, and J. Gooth, Phys. Rev. B* ***106*** *(2021) L041113,* *https://doi.org/10.1103/PhysRevB.106.L041113*

[4]* *Observation of pressure-induced Weyl state and superconductivity in a chirality-neutral Weyl semimetal candidate SrSi$_2$, M.-Y. Yao, J. Noky, Q.-G. Mu, K. Manna, N. Kumar, V. N. Strocov, C. Shekhar, S. Medvedev, Y. Sun, C. Felser, arXiv preprint (2021) arXiv:2106.11332,* *https://doi.org/10.48550/arXiv.2106.11332*

[5]* *Observation of chiral surface state in superconducting NbGe$_2$, arXiv preprint (2024) arXiv: 2403.03324,* *https://doi.org/10.48550/arXiv.2403.03324*

[6]* *Single-electron charge transfer into putative Majorana and trivial modes in individual vortices, J.-F. Ge, K. M. Bastiaans, D. Chatzopoulos, D. Cho, W. O. Tromp, T. Benschop, J. Niu, G. Gu, and M. P. Allan, Nat. Commun.* ***14*** *(2023) 3341,* *https://doi.org/10.1038/s41467-023-39109-w*

[7]* *Direct visualization of quasiparticle concentration around superconducting vortices, J. -F. Ge, K. M. Bastiaans, J. Niu, T. Benschop, M Ortego Larrazabal, M. P. Allan, arXiv preprint (2023) arXiv: 2310.05716,* *https://doi.org/10.48550/arXiv.2310.05716*

[#] jianfeng.ge@cpfs.mpg.de

[##] mengyu.yao@cpfs.mpg.de

[###] claudia.felser@cpfs.mpg.de